Detecting trihalomethanes using nanoporous-carbon coated surface-acoustic-wave sensors

Michael P. Siegal*, Curtis D. Mowry, Kent B. Pfeifer, and Dorina F. Sava Gallis

Sandia National Laboratories, Albuquerque, NM 87185

*Email: mpsiega@sandia.gov

ABSTRACT

We study nanoporous-carbon (NPC) grown via pulsed laser deposition (PLD) as a sorbent

coating on 96.5-MHz surface-acoustic-wave (SAW) devices to detect trihalomethanes (THMs),

regulated byproducts from the chemical treatment of drinking water. Using both insertion-loss

and isothermal-response measurements from known quantities of chloroform, the highest vapor

pressure THM, we optimize the NPC mass-density at 1.05 ± 0.08 g/cm³ by controlling the

background argon pressure during PLD. Precise THM quantities in a chlorobenzene solvent are

directly injected into a separation column and detected as the phase-angle shift of the SAW

device output compared to the drive signal. Using optimized NPC-coated SAWs, we study the

chloroform response as a function of operating temperatures ranging from 10-50 °C. Finally,

we demonstrate individual responses from complex mixtures of all four THMs, with masses

ranging from 10 – 2000 ng, after gas chromatography separation. Estimates for each THM

detection limit using a simple peak-height response evaluation are 4.4 ng for chloroform and 1

ng for bromoform; using an integrated-peak area response analysis improves the detection limits

to 0.73 ng for chloroform and 0.003 ng bromoform.

1

Introduction

The United States Environmental Protection Agency (US-EPA) requires all public water systems to closely monitor pathogen levels, including various bacteria, viruses, protozoa, and other organisms, which are frequently a result of fecal matter from sewage discharges, leaking septic tanks, and runoff from animal feedlots into bodies of water. Ironically, the chemical treatments of water that are critical for health, such as chlorine, bromine, ozone, or chlorine dioxide, also react in water with trace natural organic matter to create disinfection byproduct chemicals, such as trihalomethanes (THMs). THMs are a group of chlorinated and/or brominated single-carbon compounds: chloroform (CHCl₃), dichlorobromomethane (CHCl₂Br), dibromochloromethane (CHClBr₂), and bromoform (CHBr₃). The presence of THMs in the water supply was first reported in 1974. The US-EPA requires public water utilities to use treatment measures that minimize the formation of DBPs. Due to geographic and source-dependent variations, the four THMs are regulated and reported together to a maximum allowable annual average of 80 ppb (parts per billion) for total THMs.

Many methods have been reported to measure THM concentrations in water. Recently, a low-cost electrochemical technique was reported with limits of detection (LOD) of just a few ppb.² However, the authors note that the method more likely provides a measure of the total concentration of halide ions arising from all disinfection byproducts, not individual chemicals. Most methods for measuring THM concentrations in water typically have four sequential processes: purge, trap, separate, and detect. The first three are routine. Purge involves bubbling, or sparging, a gas through a specific volume of water for a sufficient period of time to extract all the volatile organic chemicals (VOCs) from the water into a gas phase. This gas flow passes through a collector, or preconcentrator, that traps VOCs but allows water vapor pass through.

The preconcentrator material is typically specific for whatever VOCs are of interest; Tenax® TA, a porous polymer resin based on 2.6-diphenylene oxide, is commonly used for THMs. Upon heating, the collector releases the trapped species that enter a separator, such as a gas chromatograph (GC). Finally a detector senses the presence of VOCs, including THMs.

A variety of detectors used in combination with GC have been reported, such as mass spectrometry (MS). GC-MS is a highly sensitive method for THM detection in water and was used to discover many disinfection byproducts in water.^{1,3} THM LODs range from several ppb to a few parts per trillion.^{4,5,6} The US EPA method using GC/MS for purgeable organic compounds has LODs for chloroform and bromoform at 0.125 and 0.2 ng per 5 mL sample.⁷ Another useful THM detector for GC is electron capture detection (ECD).⁸ Used in combination with purge and trap, GC-ECD can also achieve LODs < 1 ppb for individual THM detection; however, all of these methods require some form of sample preparation.^{9,10,11,12,13,14} Other detectors with GC have also been demonstrated, including microwave plasma emission, ¹⁵ thermal conductivity detection, ¹⁶ and atomic emission detection.¹⁷

Arrays of surface acoustic wave (SAW) device sensors were successfully demonstrated to detect a large number of VOCs, including both chloroform and bromoform at 10 ppb concentrations in water, in combination with purge and trap methods, to develop a cost-effective alternative for on-site measurement of VOCs. ¹⁸ However, detection of these low concentrations required 500 mL volume samples. Using the stated predicted capture efficiency in the paper, the best LOD for a polymer-coated SAW on a mass basis was 180 ng. In addition, using arrays of polymer-coated SAW devices requires the use of a sophisticated pattern recognition program to deconvolve the resulting data, becoming both more complex and less reliable as the number of individual VOCs present in a given sample increase. Indeed, the correct VOC classification rate

falls to 90 and 82% for binary and tertiary mixtures, respectively. ¹⁸ In addition, polymer coatings typically show aging effects with time and/or repetitive temperature cycling.

SAW sensing devices are a variation of vibrating piezoelectric crystals, first studied for gas adsorption in 1962.¹⁹ The addition of adsorbent surface coatings further improves sensitivities.²⁰ Wohltjen and Dessy advanced these concepts using 30 – 60 MHz SAW devices in 1979.²¹ SAW devices measure the mass of materials that absorb to their surface as a fundamental change in the propagation speed of a surface wave as a function of surface mass density.^{21,22,23} This effect can be observed as a shift in center frequency of the transfer function in frequency space or a phase change in the time domain.²⁴ Small shifts in the device wave propagation speed relate to the sorption of species. Sorbent coatings, such as polymers or sol gels, are used to enhance this frequency shift by allowing greater mass to adhere onto the surface.^{25,26} An effective SAW coating must be able to both sorb the desired gases and transmit an acoustic wave across its surface. This latter condition places additional requirements on an effective SAW coating. It must be sufficiently rigid to maintain the acoustic wave and have minimal residual stress such that the coating does not buckle or crack, and hence, dampen the wave. Assuming these parameters are met, there also exists a thickness constraint for a coating; too much mass will dampen a SAW, limiting the relative response to analyte sorption.

These coating requirements are met with nanoporous-carbon (NPC). NPC is a nanocrystalline form of disordered graphite that has no residual stress, is thermally stable to 600 °C, and is hydrophobic (advantageous for a water testing material since some water nearly always gets through purge, trap and separation procedures).²⁷ NPC is grown at room temperature on any substrate surface using pulsed-laser deposition. Mass density, and hence porosity and surface area, can be controlled by the deposition energetics from 2.0 g/cm³ to less than 0.1 g/cm³.

The internal structure of NPC self-assembles during growth and mainly consists of nanofragments of several aligned graphene sheets that have interplanar spacings expanded by as much as 55% compared to crystalline graphite.²⁸ Intercalation of molecules into graphite is well known. Increasing the interplanar spacing eases the diffusion of species both in and out of NPC. NPC even demonstrates a large capacity to store alkali ions for electrochemical capacitors and energy storage applications with relatively high charge and discharge rates.²⁹ More relevantly, NPC coated-SAW devices have been used to detect a large variety of VOCs, similar to the THMs. These results suggest LODs well below 1 ppb of the given saturation pressure for most of the analytes tested.³⁰

Using the results of previous study to control the resulting NPC mass density and surface area, ²⁷ here we show that NPC coatings on SAW devices can be optimized for chloroform detection near room temperature operating conditions. Note that the relatively low molecular mass and high vapor pressure of chloroform (~ 200 Torr at room temperature) make it the most difficult THM to detect for sorption-based detectors. These optimized coatings are then used to observe the dependence of chloroform detection as a function of operating temperature. Finally, we demonstrate power law response functions as well as estimate the LOD for all four individual THMs after separation by GC. This study of NPC coating feasibility for THM detection did not optimize the chromatography nor use the most sensitive measurement scheme; therefore even lower LODs are likely. These results demonstrate that NPC coated SAW sensor devices could be the basis for a relatively low-cost, reproducible, and fast-response instrument that measures individual THMs in water competitive with mass spectrometry.

Materials and Methods

NPC coatings – NPC is grown directly onto either Si or ST-cut quartz substrates between the 97 MHz Au interdigitated transducers (IDTs) of a SAW delay line using pulsed-laser deposition (PLD) as described elsewhere.²⁷ Briefly, we focus pulsed 248-nm excimer-laser radiation (KrF) to ablate a rotating pyrolytic graphite target with energy density just above the carbon ablation limit, $\sim 1.5 \text{ J/cm}^2$. With base pressure $< 10^{-7}$ Torr, we introduce a controlled pressure of Ar, ranging from p(Ar) = 100 - 180 mTorr, into the PLD vacuum chamber during growth to further attenuate the kinetic energy of the ablated species. As p(Ar) increases, the kinetic energy of the ablated species decreases, resulting in lower NPC mass densities, higher surface areas, and mechanically softer films. Using an oscillating quartz thickness monitor, each film deposition was for a constant carbon mass per unit area $\sim 0.114 \text{ mg/cm}^2$.

The depositions onto the Si substrates are used to measure the NPC mass density for each p(Ar) condition used in this study and to perform Brunauer-Emmett-Teller (BET) measurements for samples grown in p(Ar) = 140, 160, and 180 mT.³¹ Si pieces cut to 19 mm x 7.5 mm for mass density, and to 25 mm x 9 mm for BET, are weighed before and after deposition using a microbalance that records mass to tenths of micrograms. A 6.1% measurement error is based on the spread of measured NPC mass values for multiple depositions held to a constant thickness using the *in situ* monitor. Film thicknesses are determined by cleaving the NPC-coated Si(100) samples and measuring the cross-sectional film thickness using scanning electron microscopy (SEM). A 3.5% uncertainty is based on the spread of thickness measurements at different cross-sectional positions for a given sample, leading to a 7.8% uncertainty for the density determinations. Two samples were grown simultaneously at each p(Ar) for the BET experiments to generate sufficient carbon mass for the absorption studies. Note, since all of the films in this

study have similar total carbon mass deposition, lower mass density NPC films have greater thickness than higher density films. Previous study showed that low density NPC is not defined by large pores or high pore densities, but rather by a greater average interplanar spacing between graphene sheet fragments.²⁸

adsorption isotherms, the samples grown for BET measurements were dried and outgassed under vacuum at 373 K for 6 hours, using a Micromeritics ASAP 2020 surface area and porosity analyzer. Ultra-high purity N_2 (99.999%, obtained from Matheson Tri-Gas) was used in these experiments. Full adsorption and desorption N_2 isotherms up to 0.995 relative pressure (P/P₀) were measured on all samples at 77K, where P/P₀ represents the amount of nitrogen gas adsorbed onto the film at each pressure (P) relative to the saturation pressure (P₀) of nitrogen at 77K. The specific surface area was evaluated using the BET method.³¹

SAW insertion-loss characterization – The insertion-loss of each SAW device is measured before and after coating with NPC. Since a SAW delay-line device is constructed from two sets of IDTs, the band-pass characteristics of the structure resemble a $sinc^2(f-f_0)$, where f is the drive frequency and f_0 is the center frequency determined by the interdigitated finger spacing and the speed of sound in the substrate. The insertion-loss is measured at $f = f_0$ and represents the maximum power that can be transmitted through the device from the launch IDT to the receive IDT.²⁴ The measurement is made by connecting a specially designed SAW fixture to an HP-8753D network analyzer programmed to make an S12 measurement.

In a SAW device, acoustic energy probes the surface of the substrate between the two IDTs: the insertion-loss measurement can therefore be used as a diagnostic tool to evaluate the quality of a given film deposited on the SAW device. Material coatings on the SAW device surface increase the insertion-loss depending on the thickness and stiffness of the film. For example, an elastomeric film will increase the SAW device insertion-loss due to energy transfer into the film from the substrate that is subsequently dissipated by the film. Similarly, a low mass-density film will have inelastic behavior that increases the film insertion loss. In contrast, a rigid film will move in synchronous motion with the substrate absorbing very little of the wave energy and producing small losses in the SAW.³² Since the total carbon mass per unit area is constant for each NPC deposition, two devices with similar total mass but different mass density can be differentiated using the insertion loss.

SAW sensing mechanism – A SAW device measures the presence of a chemical analyte by detecting a change in the speed of the acoustic wave traveling across the device surface as material is loaded onto that surface. A chemically sensitive film will absorb analyte from the atmosphere and increase the film mass, reducing the acoustic wave speed. There are two common methods of using a sensor system based on this phenomenon: fixed phase/variable frequency and fixed frequency/variable phase. The first uses the SAW device as the feedback element in an oscillator circuit and is extensively described in the literature. 33,34,35,36,37,38

The second method drives a SAW device at a fixed frequency (nominally the minimum insertion-loss frequency) and compares the phase-angle shift of the device output to the phase-angle of the drive signal. The phase-angle varies with the speed of sound in the device. We use this approach to perform analyte detection measurements with a network analyzer; however, this

can be done using a simple and inexpensive phase measurement circuit that outputs an analog signal representing the phase-shift.^{39,40}

THM analyte characterization – We tested the absorption properties of the NPC-coated SAW devices by injecting into a separation column precise quantities of either chloroform alone or mixtures of all four THMs simultaneously: chloroform (CF), dichlorobromomethane (DCBM), dibromochloromethane (DBCM), and bromoform (BF). Standard solutions were prepared using individual THMs as gravimetric serial dilutions using a chlorobenzene solvent.

The SAW devices were designed and fabricated to have a fundamental frequency near 96.5 MHz. The insertion loss of a typical uncoated SAW device used in this study is -10.5 dB ± 0.3 dB. The NPC-coated SAW sensors are kept in a gas-tight brass enclosure using gold spring-loaded contacts. The brass enclosure was held in an aluminum block in thermal contact to a flow-through chilled-water fixture. The entire fixture was operated inside a gas chromatography oven to maintain a constant temperature during testing, ranging between 10 and 50 °C, as measured within the aluminum block. A network analyzer monitored the phase response of the SAW device while sweeping a 1 MHz span centered at the target frequency. Chemical response is detected by monitoring the phase-angle versus time at a center-frequency determined during the insertion-loss measurements, i.e. the frequency of least attenuation for a given device. This is typically within a few hundred Hz of the target 96.5 MHz and can vary somewhat based on SAW manufacture. The network analyzer phase signal was recorded versus time.

A tandem gas chromatograph configuration allowed for different temperature conditions for the chemical separation and the SAW device. We used an autosampler to inject $0.2 \,\mu l$ of each chemical standard into a separation column (10 m long, 0.25 mm inner diameter, DB-624

phase, $1.4 \,\mu m$ thick) held isothermally at 75 °C and transited a constant temperature tube (Clayborn Lab, Truckee, CA, hot tube) held at 130 °C into the second GC oven held at 40 °C. The GC conditions were not optimized for narrowest peak width, but were an instrumental compromise to enable short analysis times. The SAW detector for mixed THM samples was 25 °C, unless otherwise noted. A "Deans switch" (Agilent, Santa Clara, CA, model #G2855b) was used to change the column flow to backflush solvent to waste, preventing solvent from reaching the SAW device. While chlorobenzene harms neither the SAW device nor the NPC coating, this procedure increases sample throughput by eliminating the time required to clear the solvent through the chromatography chain. The quantity of each THM standard reaching the SAW, in nanograms, is determined by adjusting the mass injected by the total split ratio. This is calculated by dividing the detector flow by the total flow that includes the detector flow, split vent, purge vent, and dean switch exit flows. N_2 (99.9995%, Trigas Corp, Albuquerque, NM) was used as the carrier gas; however, any unreactive gas, such as He, can also be used.

Results and Discussion

NPC mass density study – Using a constant 1.5 J/cm² laser energy density to ablate the pyrolytic graphite target during PLD controls the resulting NPC mass density. Increasing p(Ar) lowers the kinetic energy of the ablated carbon species via collisions with Ar atoms as it travels from the target to the growth substrates, resulting in lower NPC mass density. NPC films grown on Si(100) substrates were used to determine the resulting mass density for films grown in p(Ar) ranging from 120 – 170 mT. The *in situ* oscillating quartz thickness monitor was not responsive for films grown in $p(Ar) \ge 180$ mT, hence we limited this study to films deposited in $p(Ar) \le 170$ mT. We deposited each film to the same total areal mass ~ 0.114 mg/cm². NPC mass was

accurately measured by weighing the substrates before and after deposition using a Mettler microbalance. Film thickness was measured in an SEM. With NPC film thickness, area, and mass each measured, the mass densities are easily determined and are plotted in Figure 1 as a function of the Ar total pressure in the PLD chamber during NPC film growth. Taking the error bars into account, the NPC mass density ranges from 1.6 to 0.86 g/cm³ when grown in p(Ar) ranging from 120 to 170 mT, respectively.

BET specific surface area results – Samples for BET characterization were grown at 140, 160 and 180 mT, and have mass densities of 1.27, 0.98, and 0.90 g/cm³, respectively. Only the masses of the NPC films were considered in the BET specific surface area measurements calculations; all substrate contributions are considered negligible and were excluded. The nitrogen adsorption isotherm at 77 K for each NPC sample is shown in Fig. 2(a). The shapes of these curves are similar to those reported elsewhere for various types of carbon nanotubes, another pure sp² carbon bonded material.⁴¹ A standard BET measurement requires at least 3 points to fit a linear plot, in a P/P_0 range of 0.05 to 0.35 on a nitrogen adsorption isotherm.⁴² In these experiments, the best fits were obtained in 0.07-0.21 P/P₀ range. Fig. 2(b) shows the calculated BET surface areas and finds that they are inversely proportional to NPC mass density: $997 \pm 32 \text{ m}^2/\text{g}$, $1262 \pm 29 \text{ m}^2/\text{g}$ and $1339 \pm 29 \text{ m}^2/\text{g}$ for samples with mass densities of 1.27, 0.98, and 0.90 g/cm³, respectively. Such values are typical of those reported for various other carbon materials. For example, while the surface area of a single graphene sheet is 2630 m²/g, chemically-modified graphene agglomerates used for graphene-based ultracapacitors report a BET surface area of only $705 \text{ m}^2/\text{g}$. Ordered mesoporous carbons have $1500 - 1800 \text{ m}^2/\text{g}$ surface areas. 44 Carbon nanotube bundles have BET surface areas ranging from 200 – 600 m²/g

depending on tube diameters and other structural characteristics.⁴¹ Finally, we previously reported very low NPC mass densities that should have significantly higher BET surface areas.²⁷ However, such coatings are not optimal for SAW performance due to large insertion losses, as discussed below.

Insertion loss characterization – As NPC mass density is reduced and the material becomes mechanically softer, it becomes more difficult to pass an acoustic wave across its surface, leading to higher SAW device insertion-losses. This is shown in Figure 3 for NPC coatings deposited on two SAW devices each in p(Ar) ranging from 140 to 180 mT. Note that the high insertion losses measured for SAWs coated in p(Ar) = 180 mT coincide with the condition that also limited the responsiveness of our *in situ* oscillating quartz crystal thickness monitor during PLD growth. The insert shows an expanded view of the insertion-loss for NPC coatings deposited in $p(Ar) \le 170$ mT. This expanded plot shows that insertion-loss actually begins to sharply increase for NPC deposited in p(Ar) > 160 mT inferring that the insertion loss is highly sensitive to variations in film stiffness resulting from falling below a critical mass density ~ 0.98 g/cm³. Films grown in this high slope region suggest the potential degradation of reliability and reproducibility of the coatings for SAW performance. While the consequences of operating with high and varying insertion loss SAW devices have not been exhaustively studied, for this investigation, we choose to minimize the insertion loss uncertainty by limiting our samples to devices with less than -3dB additional insertion loss over the uncoated devices.

SAW performance vs. NPC deposition condition/mass density – SAWs coated with NPC films deposited in p(Ar) from 100 – 170 mT were tested for sensitivity to detect CF exposures ranging from 10 – 2000 ng. Fig. 4 shows the results for NPC films deposited in p(Ar) ranging

from 140 – 170 mT, where the vertical axis is the total integrated area under the phase-shift response peak. Prior work found that the SAW response to analyte concentration follows a power-law f unction that fits a straight line fit when plotted on a log-log scale.^{28,30} Figure 4 shows that this functionality is followed for the NPC films grown in $p(Ar) \ge 150$ mT; however, NPC films grown in p(Ar) = 140 mT show a curved response. Not shown are data for NPC films grown in p(Ar) = 100 and 120 mT, where this downward curvature at the lower CF mass injections is even more pronounced. These results imply that NPC coatings deposited in conditions that lead to mass densities ≥ 1.27 g/cm³ will not be as sensitive to low analyte doses as coatings deposited in higher p(Ar).²⁷ Recall, that there does not appear to be any variation in nanopore size or concentration as a function of NPC mass density, but rather a significant change in the average interplanar spacing between graphene sheet fragments.²⁸ We infer that NPC with densities ≥ 1.27 g/cm³ have interplanar spacings sufficiently small such that the diffusion rate of CF into NPC decreases, especially for the smallest mass exposures, reducing the SAW response to a given injected dose. This is also related to the BET measured decrease in surface areas for NPC with higher density.

Conversely, NPC films with densities ≤ 1.12 g/cm³ have higher BET surface areas and appear to have interplanar spacings between the graphene sheet fragments sufficiently large such that analytes can readily diffuse into the structure, even for the lowest CF mass injections studied.

However, the results presented in Fig. 3 shows that NPC films with low mass densities $< 0.94 \text{ g/cm}^3$ grown in p(Ar) > 170 mT begin to have uncontrolled high insertion losses that could affect the SAW response signal-to-noise ratio. In combination, these results set a reasonable window for the growth of highly-sensitive NPC coatings on SAW devices to those deposited in p(Ar) ranging from 150 - 160 mT, resulting in mass densities ranging from 0.98 - 1.12. Hence,

we used NPC films deposited in p(Ar) = 155 mT, with mass density $\sim 1.05 \pm 0.08$ g/cm³, for the remainder of this study.

NPC-coated SAW device performance vs. temperature – Sensor performance as a function of operating temperature is an important consideration for applications. Figure 5 shows the peak response of a SAW device coated with the optimal NPC mass density (~ 1.05 g/cm³) as a function of injected CF mass, operating at temperatures ranging from 10 – 50 °C. Note that this data is plotted simply as the maximum phase angle shift in the response signal, rather than the integrated area under the peak. Either method for evaluation can be used, although integrating the area under the peaks provides improved signal-to-noise, as will be seen below for the THM LOD determinations. Not surprisingly, low-temperature operation of a SAW sensor device is more sensitive to CF than high-temperature operation. As the operating temperature increases, the corresponding higher analyte vapor pressure decreases the amount of gas that can be sorbed into the NPC coating, resulting in a smaller phase shift response to a given mass injection of analyte.

The dashed horizontal line at the bottom of the plot represents triple the value of the smallest measureable phase shift response of the NPC-coated SAW device with our electronic instrumentation. With a SAW device of ~ 13 dB insertion loss, the estimated standard deviation in the phase angle, based on instrumentation noise in the HP-8753D network analyzer at room temperature, is on the order of $\sigma = 0.07^{\circ}$. Therefore, the commonly-used 3σ LOD calculation allows us to extrapolate the power law behavior to $\sim 0.21^{\circ}$ phase shift. In reality, we are extrapolating to $\sim 0.25^{\circ}$ which is a cutoff near 4σ . Hence, we consider this a conservative approximate estimate of the LOD for the peak SAW response data.

The intersection of the power-law extrapolations with the detection-limit provides an estimated LOD for this NPC-coated SAW device. Note that in Fig. 4 the power law is an excellent fit to 6 injected masses over a much wider range, including values near 10 ng, or in the middle of the four LOD intersections presented here, further demonstrating that such low detectability exists. The Fig. 5 inset plots the CF LOD and shows that it varies exponentially with temperature, ranging from 3.5 - 30 ng at $10 \,^{\circ}\text{C} - 50 \,^{\circ}\text{C}$, respectively. This dependence of signal response to the operating temperature is expected, resulting from the Clausius-Clapeyron equation describing vapor pressure as an exponential function of temperature.

Determining THM limits-of-detection – All four THMs are measured simultaneously by injecting quantified mixed solutions into the GC column at 24.5 °C for chemical separation. The individual THM concentrations for each solution are listed in Table I. The effluent is measured with an NPC-coated SAW device as a function of GC retention time. Each mixed solution is measured twice. (Note that a slightly thicker NPC coating of 0.13 mg/cm² was used for this experiment and is responsible for the somewhat higher phase angle responses than the coated SAWS used to study both the NPC mass density and temperature of operation for CF detection.) The results are shown in Figure 6(a). Figure 6(b) is an expanded view of the testing performed for the lowest THM concentration solution. The THMs are released from the GC in order of their molecular weights, which also correspond to their boiling points. Therefore, CF is released first from the GC column, followed by DCBM, then DBCM, and finally BF.

Fig. 6 can be analyzed two different ways to quantify the SAW sensor response for each THM as a function of its total injected mass. The first and simplest method uses the maximum

SAW phase shift, similar to that used in Fig. 5. This is plotted in Fig. 7(a) for each THM peak in Fig. 6. The thick dashed lines through the data points are a best fit to a power-law function. To measure the LOD for each THM, the minimum SAW response above the noise level must be determined. This is estimated using Fig. 6(b). The noise-level, i.e. the peak thickness of the baseline level, is approximately 0.15° with a standard deviation of ± 0.07°. A SAW response to a given analyte mass injection that is three times the standard deviation of the noise level is again defined as a reliable detection limit, therefore setting this instrumentation limit to 0.21° above the baseline, shown as a dashed horizontal line in Fig. 7(a). The intersection of the thin lines extrapolated from the power-law fits to this detection limit provides an estimated LOD for each individual THM studied. The LODs for CF, DCBM, DBCM, and BF are 4.4, 1.5, 1.1, and 1.0 ng, respectively, and are listed in Table II.

A second, and more accurate method, to analyze SAW responses to analyte exposures is to integrate the total area under each response peak.^{9·10·12·13·14·17} The integrated peak areas are plotted against the known injected analyte mass for each THM in Fig. 7(b). Compared to using the simple peak-height analysis in Fig. 7(a), note that the integrated peak responses for each THM are relatively parallel to one another, indicating that they all follow a similar power-law behavior. This implies that the LOD for BF will be significantly lower than that of DCBM using this methodology, which is expected given its much larger total area signal observed in Fig. 6(b).

To estimate the LOD of each THM using the integrated peak area method, the 3σ response of the SAW device noise level must be determined. Again, this is estimated by using the CF response in Fig. 6(b). The same height above the noise level will be required to definitively observe a response; however, the width of the peak can be much narrower. Here the CF response is ~ 8 s wide. Clearly a peak ≤ 1 s wide will still be observable. Indeed, this is

likely well above the true limit of observation. The 3σ integrated peak response is ~ 0.21 deg•s, shown as a dashed horizontal line in Fig. 7(b). The estimated LODs for CF, DCBM, DBCM, and BF are 0.73, 0.18, 0.006, and 0.003 ng, respectively, and are listed in Table II.

Table II summarizes the injected THM mass LODs estimates using an NPC-coated SAW device sensor for GC analysis, for both the simple peak height method, as well as the more highly-sensitive peak area method. The lower estimated LODs from the peak height area method are not surprising considering the larger data sampling available for integration. Nevertheless, even the simple peak-height analysis results in LODs of 4 and 1 ng for CF and BF, respectively, comparing very favorably to electrochemical analysis with LODs of 60 and 30 ng for CF and BF, respectively, after adjusting for their reported water sampling size of 10 mL.² GC-ECD reports LODs of $0.9 \mu g/L$ for both CF and BF in 100 mL water samples, corresponding to 90 ng LODs.¹⁴ Indeed, the estimated individual LODs determined in this work are comparable to more complex and more expensive GC-MS apparatus. The LODs listed for CF and BF in EPA method 524.3, using a 5 mL sample for purgeable organics by GC/MS are 0.025 and $0.040 \mu g/L$ which correspond to 0.125 and 0.2 ng on a mass basis.⁷

Conclusions

Nanoporous-carbon is an effective sorbent coating on SAW sensor devices for the detection of trihalomethanes. The effectiveness of NPC is a function of its optimal mass density together with a high BET surface area, simultaneously combining to provide a material with high surface area to absorb analytes and sufficient stiffness to enable low loss surface acoustic wave transmission. Using the insertion loss behavior of coated SAW devices helps set a lower bound for an acceptable NPC mass density. The onset of deviations from a power law behavior for

analyte detection as a function of inserted analyte mass sets the upper bound for acceptable NPC mass density. Using these criteria, we find that NPC mass densities between 0.9 and 1.1 g/cm³ provide optimal SAW sensor performance for chloroform. Using NPC coatings with mass density ~ 1.05 g/cm³, we studied the effect of operating temperature on SAW sensing performance for chloroform and estimate the CF LOD to range exponentially from 3.5-30 ng from 10-50 °C, respectively. Such LODs should be sufficient to detect CF in water to even lower values compared to other reported methods in the literature, taking into account the size of a given water sample to be sparged.

Finally, we demonstrated that GC can separate complex mixtures of all four THMs for measurement by an NPC-coated SAW sensor device in ~ 3 minutes. The resulting data can be analyzed either by measuring the maximum SAW phase angle response for each THM, or more accurately by integrating the area under each THM peak. Both methods result in isotherms for each THM that follow power law behaviors. The estimated LODs for NPC-coated SAW devices are 4.0, 1.5, 1.1 and 1.0 ng using the peak height method, and 0.73, 0.18, 0.006 and 0.003 ng using the peak area method, for CF, DCBM, DBCM and BF, respectively. These LODs are among the very lowest ever reported for individual THM detection.

Acknowledgements

The authors thank Don Overmyer for growing the NPC films on SAW devices, Jonathan Rivera for growing the NPC films for the mass density measurements, Lyle Brunke for growing the films for BET characterization, Art Rumpf for insertion-loss characterization, Stephen Howell for data acquisition and Labview[™] software, and Richard Kottenstette and Alex Robinson for analyte measurements. This work is supported in part by the Laboratory Directed Research and Development program at Sandia National Laboratories. Sandia National Laboratories is a multiprogram laboratory managed and operated by Sandia Corporation, a wholly owned subsidiary of Lockheed Martin Company, for the U.S. Department of Energy's National Nuclear Security Administration under Contract DE-AC04-94AL85000.

Table I Concentration of each THM in the four solutions used for testing in Fig. 4

THM	A [ng]	B [ng]	C [ng]	D [ng]
CF	14.2	85.7	954	1860
DCBM	13.9	82.1	926	1812
DBCM	14.3	111	920	1864
BF	13.0	108	909	1815

Table II

THM LODs using an NPC-coated SAW device sensor

THM	CF	DCBM	DBCM	BF
Peak Ht. LOD [ng]	4.4	1.5	1.1	1.0
Int. Area LOD [ng]	0.73	0.18	0.006	0.003

Figure Captions

- **Fig. 1.** The variation of NPC mass density as a function of the PLD p(Ar) used during film growth. The dashed line provides a guide to the eye.
- **Fig. 2.** (a) N_2 absorption isotherms at 77 K for NPC films grown using different p(Ar). (b) NPC surface area calculated from curves in (a) using the BET method as a function of NPC mass density.
- **Fig. 3.** Insertion loss of a SAW device after coating with an NPC film as a function of the p(Ar) used during NPC deposition. Inset: Expanded view.
- **Fig. 4.** The integrated peak area response of SAW devices each coated with 0.1 mg/cm² NPC under different p(Ar) vs. injected known CF mass.
- **Fig. 5.** The peak response for an optimal mass density NPC-coated SAW device vs. controlled CF mass injections for various operating temperatures. The dashed line represents the phase angle response that is 3σ the instrumentation limits. Inset: The extrapolated CF LODs as a function of operating temperature.
- **Fig. 6.** (a) The response of a SAW device coated with 0.13 mg/cm² NPC to each THM at the injected masses listed in Table I. Each solution is measure twice. (b) An expanded view of the response from both tests of mixture "A", the lowest THM injected mass solution.
- Fig. 7. Analysis of the NPC-coated SAW sensor responses to THM injected masses using (a) the maximum phase shift for detecting each analyte, and (b) the integrated area under the phase shift response for each analyte. The thick dashed lines are a best fit to a power law function. The thin line extensions are extrapolations to values 3σ the instrumentation limits, which are represented by the horizontal dashed lines.

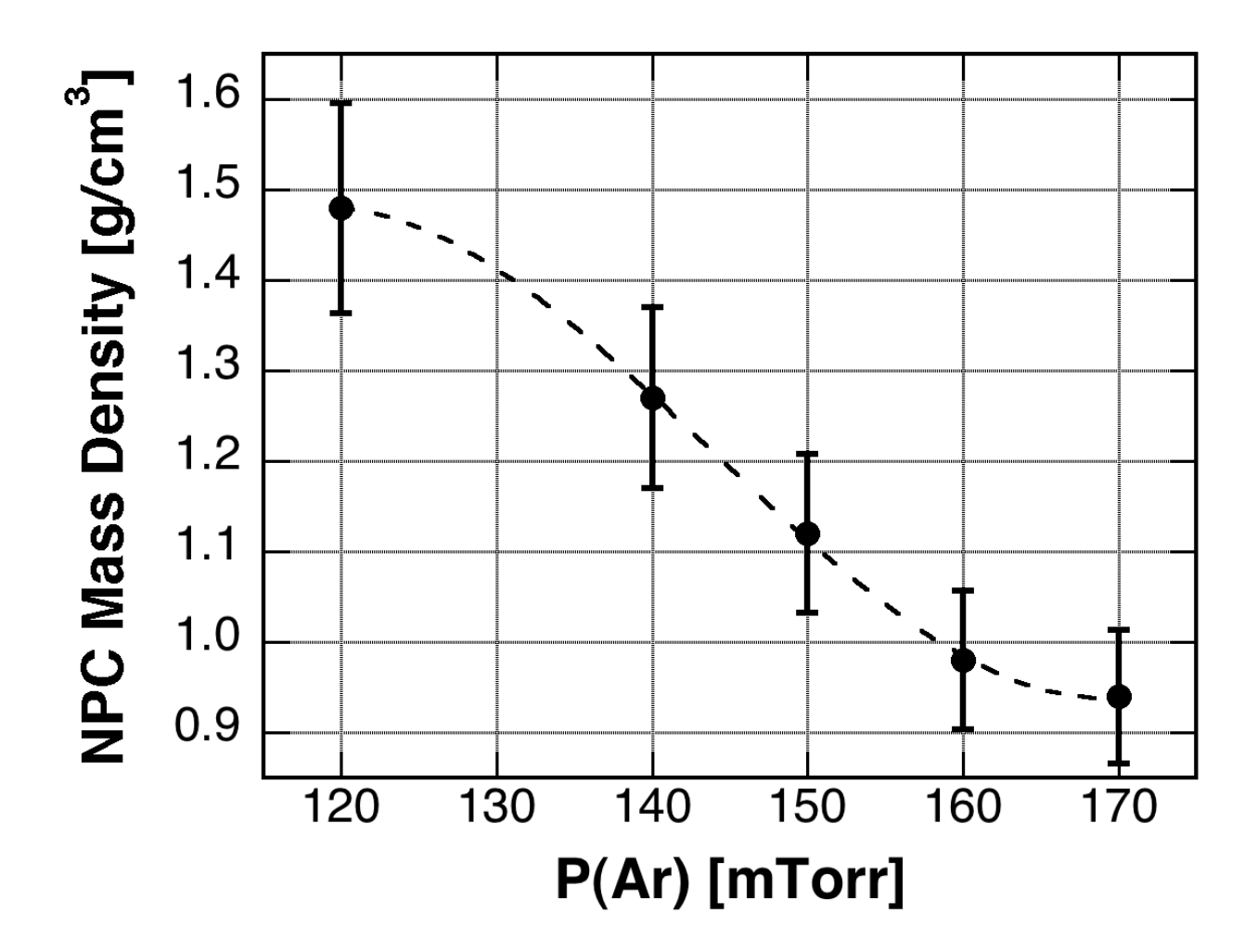
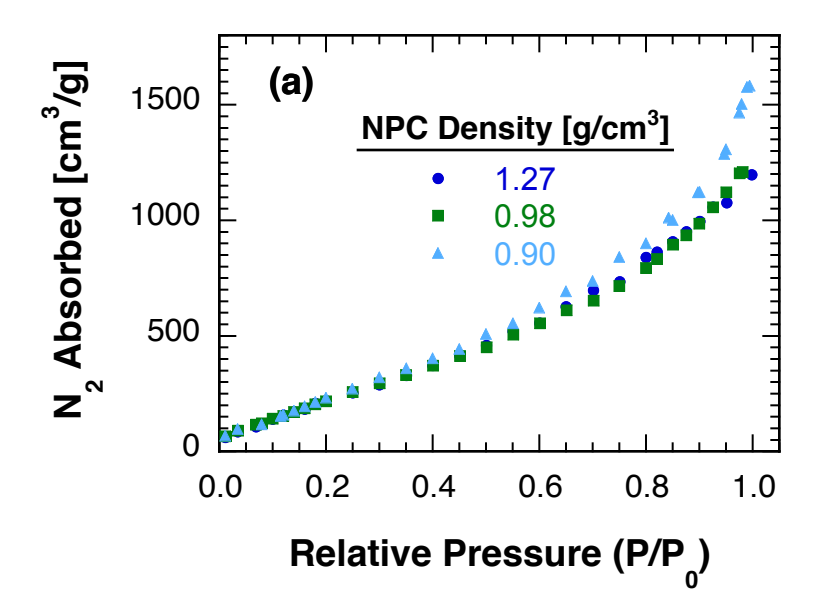


Figure 1



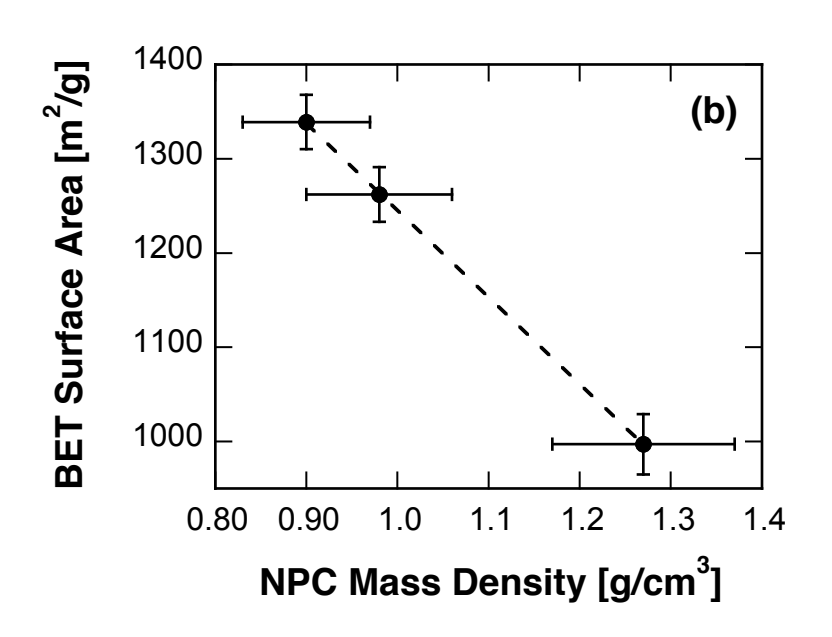


Figure 2

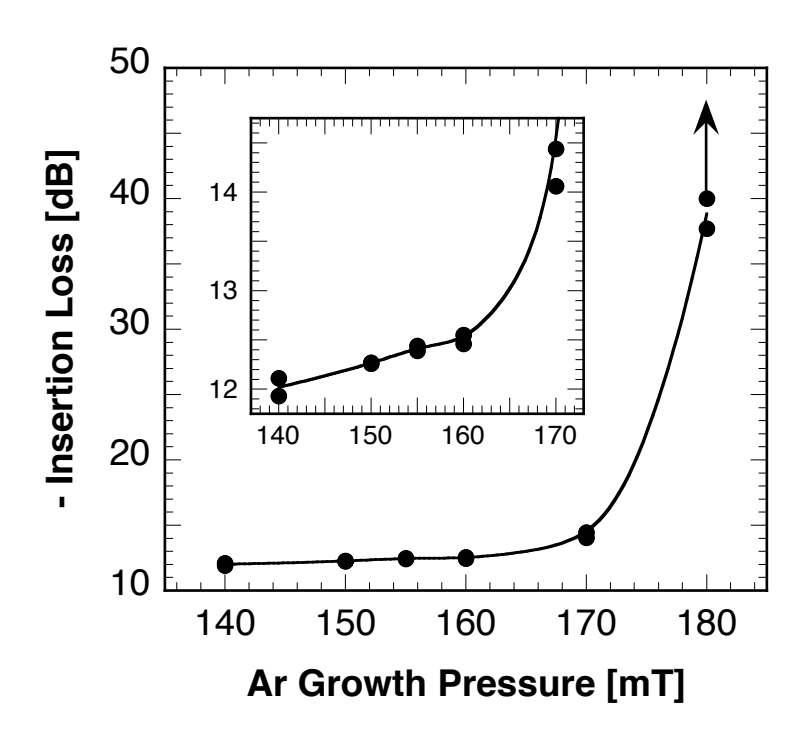


Figure 3

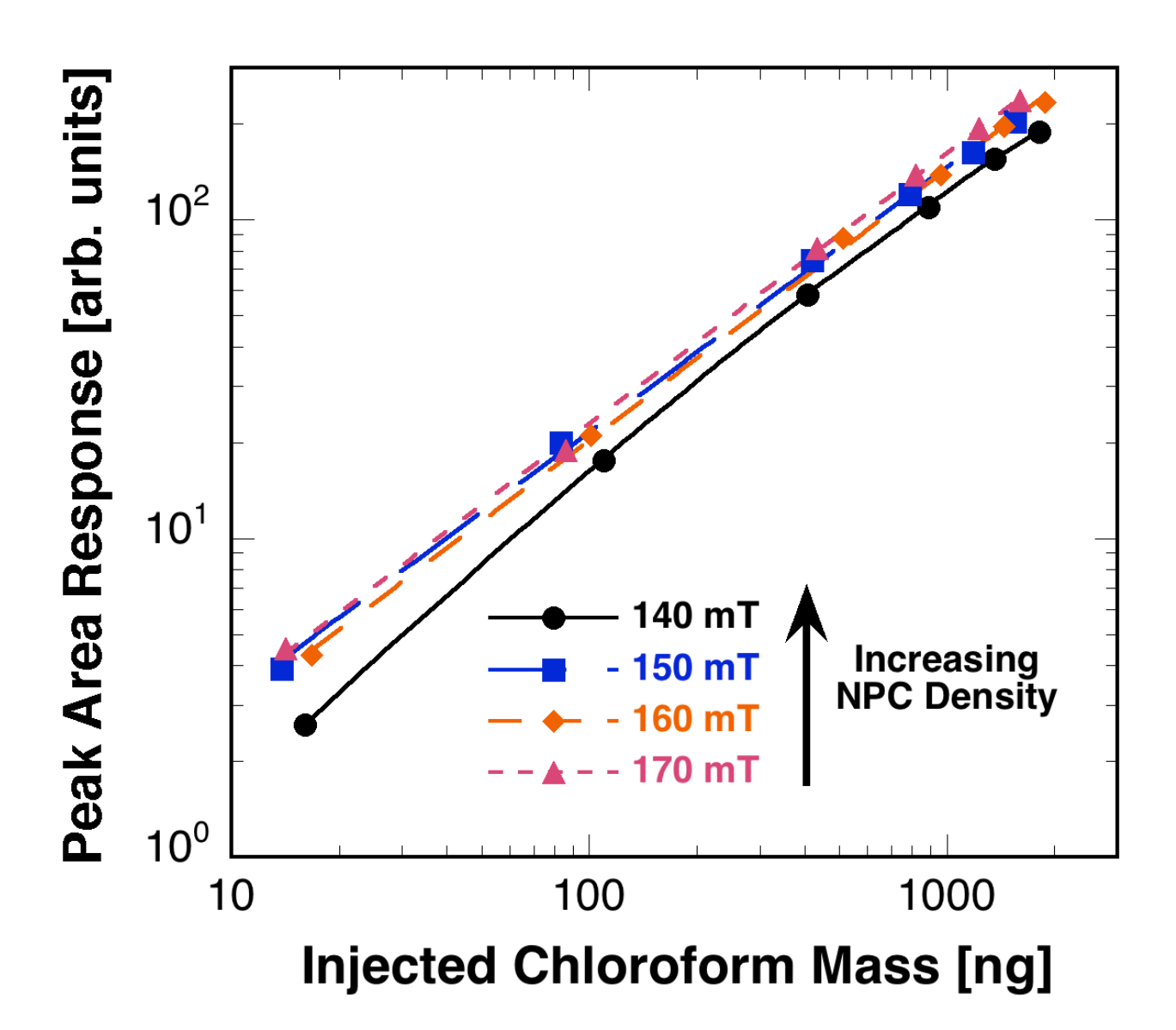


Figure 4

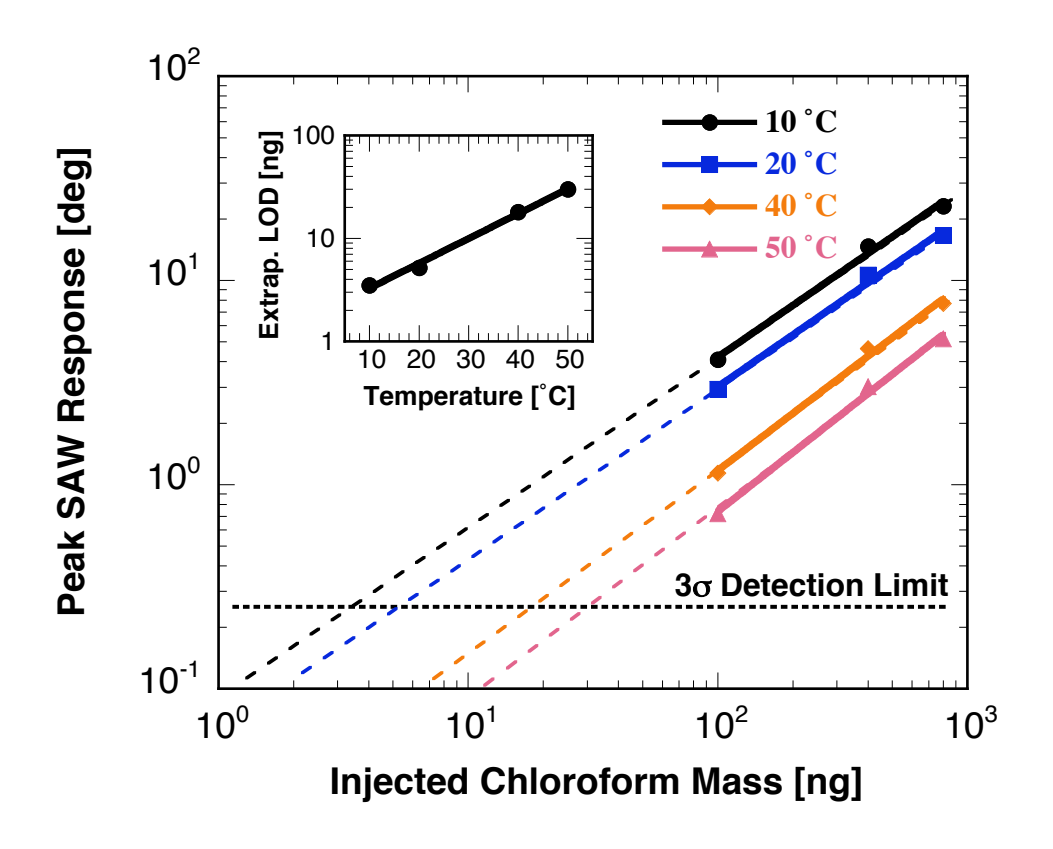


Figure 5

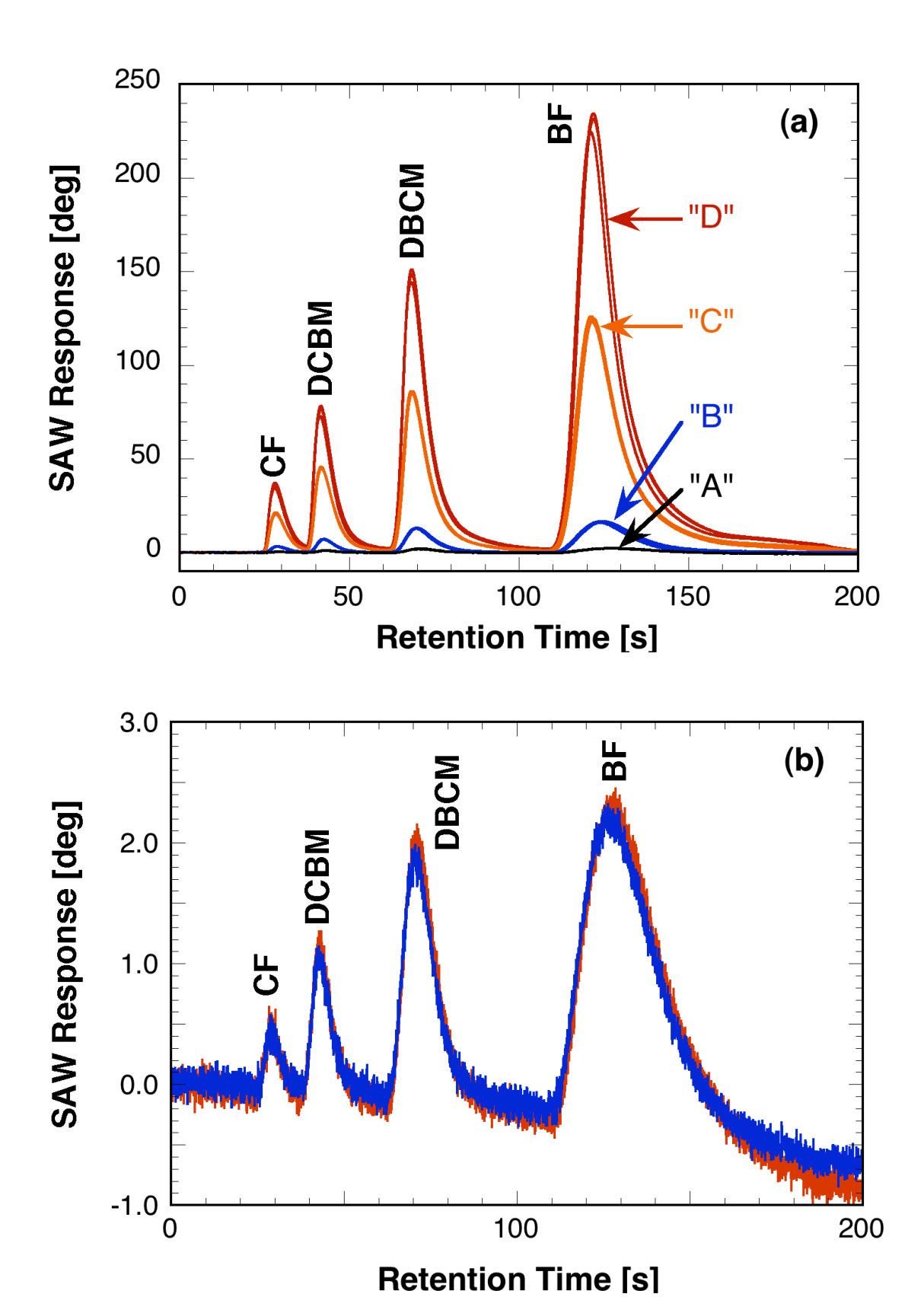
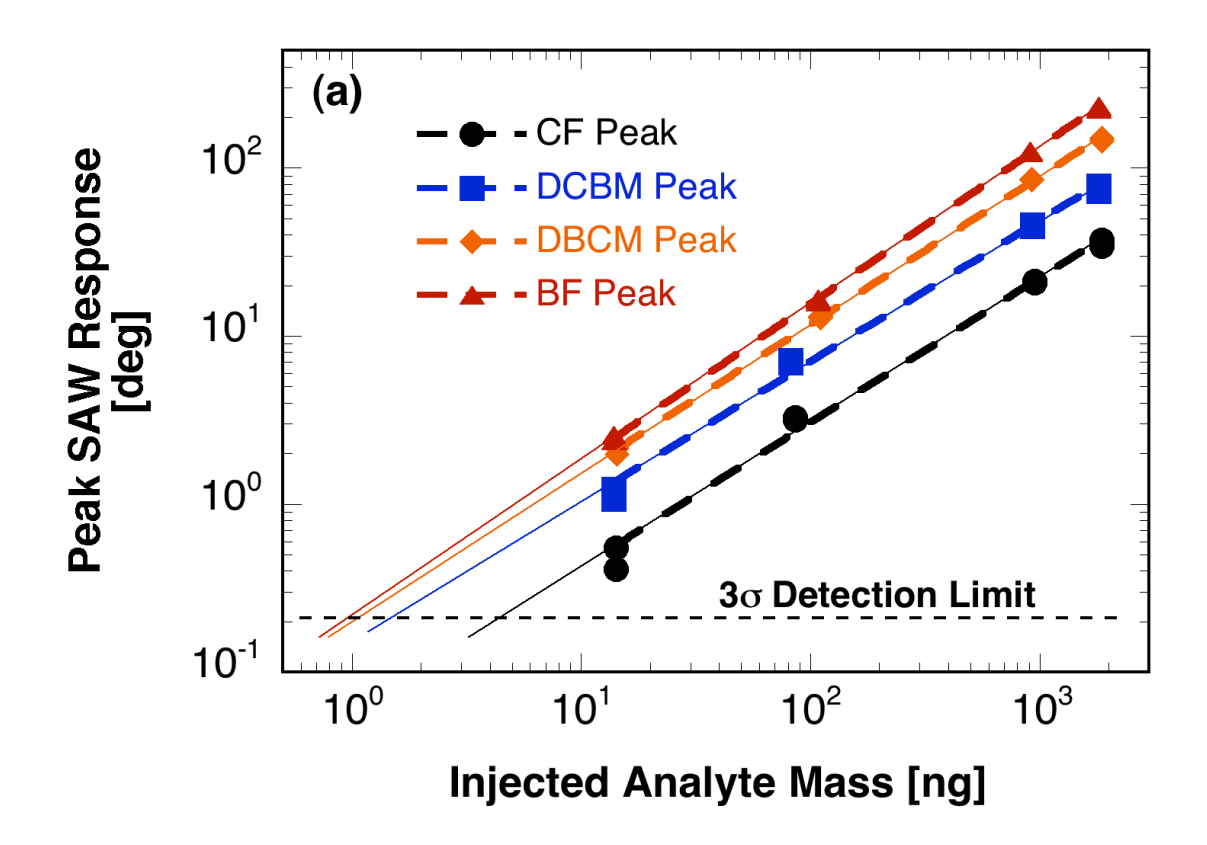


Figure 6



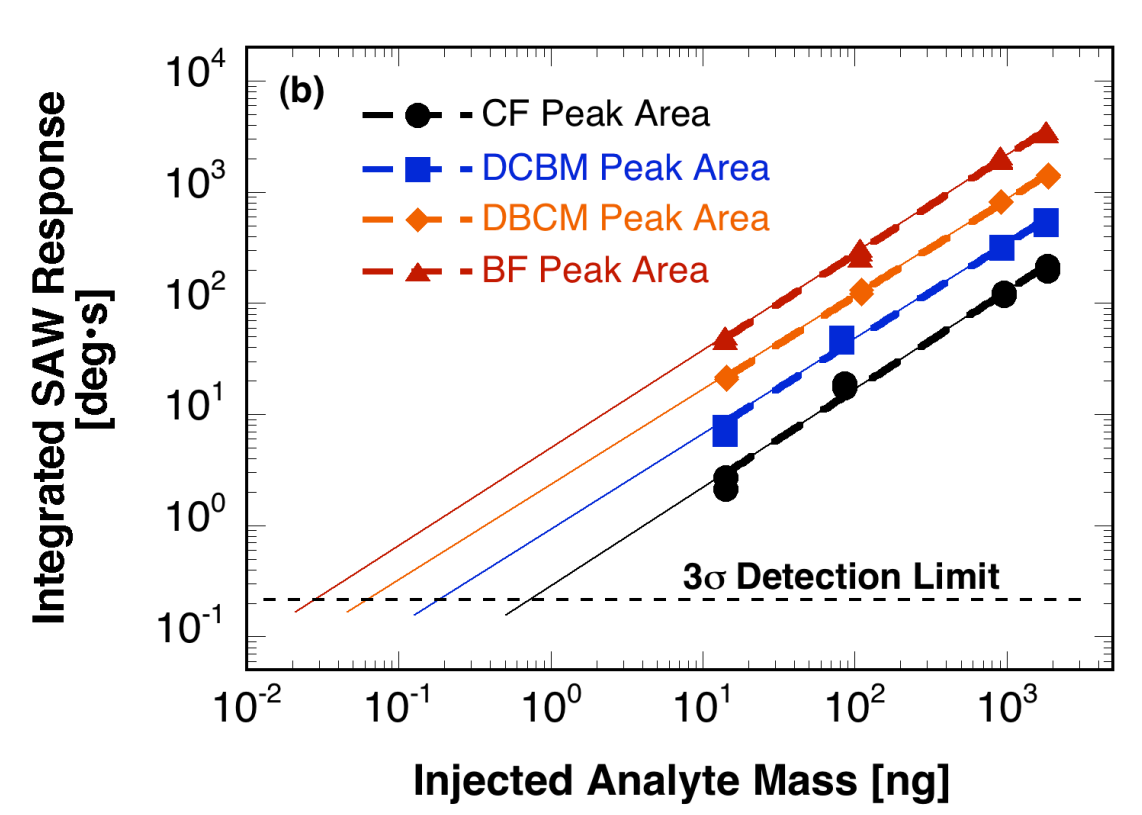


Figure 7

References

¹ J. J. Rook, *Water. Treat. Exam.*, **23**, 234 (2002).

- ⁵ M. A. Jochman, X. Yuan, and T. C. Schmidt, *Anal. Bioanal. Chem.*, **387**, 2163 (2007).
- E. Aguilera-Herrador, R. Lucena, S. Cardenas, M. and Valcarcel, *J. Chroma. A.*, **1209**, 76 (2008).
- B. Prakash, A. D. Zaffiro, M. Zimmerman, D. J. Munch, and and B. V. Pepich, *Method*524.3: Measurement Of Purgeable Organic Compounds In Water By Capillary Column Gas

 Chromatography/Mass Spectrometry ver. 1.0. Office of Ground Water and Drinking Water,

 U.S. Environmental Protection Agency: Cincinnati, Ohio, (2009).
- ⁸ T. Aoki and K. Kawakami, *Water Res.*, **23**, 739 (1989).
- ⁹ L. Lepine and J.-F. Archambault, *Anal. Chem.*, **64**, 810 (1992).
- D.-H. Cho, S.-H. Kong, and S.-G. Oh, *Water Res.*, **37**, 402 (2003).
- ¹¹ M. Y. Tominaga and A. F. Midio, *Braz. J. Pharm. Sci.*, **37**, 195 (2003).
- ¹² R.-S. Zhao, W.-J. Lao and X.-B. Xu, *Talanta*, **62**, 751 (2004).
- ¹³ G. L. Emmert, G. Cao, C. Duty, and W. Wolcott, *Talanta*, **63**, 675 (2004).
- ¹⁴ M. A. Brown and G. L. Emmert, *Anal. Chim. Acta*, **555**, 75 (2006).
- ¹⁵ B. D. Quimby, M. F. Delaney, P. C. Uden, and R. M. Barnes, *Anal. Chem.*, **7**, 875 (1979).
- ¹⁶ A. Segal, T. Gorecki, P. Mussche, J. Lips, and J. Pawliszyn, J. Chromat. A, 873, 13 (2000).

² A. A. Peverly, and D. G. Peters, *Anal. Chem.*, **84**, 6110 (2012).

³ S. D. Richardson, *J. Environ. Monit.*, **4**, 1 (2002).

⁴ L. Zoccolillo, L. Amendola, C. Cafaro, and S. Insogna, J. Chroma. A., 1077, 181 (2005).

- N. Campillo, P. Vinas, I. Lopez-Garcia, N. Aguinaga, and M. Hernadez-Cordoba, *J. Chromat.*A, 1035, 1 (2004).
- W. A. Groves, A. B. Grey, and P. T. O'Shaugnessy, *J. Envior. Monit.*, **8**, 932 (2006).
- ¹⁹ L. J. Slutsky and W. H. Wade, *J. Chem. Phys.*, **36**, 2688 (1962).
- ²⁰ V. N. Smith and J. F. Fidiam, *Anal. Chem.*, **36**, 1735 (1964).
- ²¹ H. Wohltjen and R. Dessy, *Anal. Chem.*, **51**, 1458, 1465, 1475 (1979).
- ²² H. Wohltjen, *Anal. Chem.*, **56**, 87A (1984).
- ²³ R. C. Hughes, A. J. Ricco, M. A. Butler, and S. J. Martin, *Science*, **254**, 74 (1991).
- D. S. Ballantine, R. M. White, S. J. Martin, A. J. Ricco, G. C. Frye, E. T. Zellers, and H. Wohltjen, *Acoustic Wave Sensors: Theory, Design, and Physico-Chemical Applications*, San Diego, CA, Academic Press, 1997, pp. 77-79.
- ²⁵ A. J. Ricco, G. C. Frye, and S. J. Martin, *Langmuir*, **5**, 273 (1989).
- ²⁶ R. C. Thomas, L. Sun, R. M. Crooks, and A. J. Ricco, *Langmuir*, 7, 620 (1991).
- M. P. Siegal, D. L. Overmyer, R. J. Kottenstette, D. R. Tallant, and W. G. Yelton, *Appl. Phys. Lett.* **80**, 3940 (2002).
- ²⁸ M. P. Siegal, W. G. Yelton, D. L. Overmyer, and P. P. Provencio, *Langmuir*, **20**, **1194** (2002).
- S. J. Limmer, W. G. Yelton, M. P. Siegal, and B. C. Bunker, *Electrochem. Soc. Trans.*, **28**, 89 (2010).
- ³⁰ M. P. Siegal and W. G. Yelton, *Adv. Sci. Technol.*, **48**, 161 (2006).
- S. Brunauer, P. H. Emmett, E. Teller, *J. Am. Chem. Soc.*, **60**, 309 (1938).
- ³² S. J. Martin, G. C. Frye, and S. D. Senturia, *Anal. Chem.*, **66**, 2201 (1994).
- D.-B. Seo, C. Chicone, and Z. C. Feng, Sensors and Actuators A, 121, 44 (2005).
- ³⁴ Z. C. Feng and C. Chicone, *Sensors and Actuators A*, **104**, 171 (2003).

³⁵ K. B. Pfeifer, *Langmuir*, **11**, 4793 (1995).

- H. Wohltjen, A. W. Snow, W. R. Barger, and D. S. Ballantine, *IEEE Trans. on Ultrasonics*, *Ferroelectrics*, and *Frequency Control*, **34**, 172 (1987).
- A. J. Ricco, S. J. Martin, and T. E. Zipperian, Sensors and Actuators, 8, 319 (1985).
- ³⁸ K. B. Pfeifer, J. L. Sprung, and T. R. Galloway, Sensors and Actuators B, 22, 37 (1994).
- N. Ramakrishnan, H. B. Nemade, and R. P. Palathinkal, *IEEE Sensors Journal*, **11**, 430 (2011).
- R. W. Cernosek, A. N. Rumpf, G. J. Sanchez, C. K. Wojahn, and R. Pohl, *in Chemical Sensors IV*, M. Butler, N. Yamazoe, P. Vanysek, and M. Aizawa, Editors, PV 99, p. 355, The Electrochemical Society Proceedings Series, Pennington, NJ (1999).
- ⁴¹ F. Li, Y. Wang, D. Wang, and F. Wei, *Carbon*, **42**, 2375 (2004).
- S. Lowell, J.E. Shields, M.A. Thomas, M. Thommes, in "Characterization of Porous Solids and Powders: Surface Area, Pore Size and Density", Kluwer Academic Publisher, Dordrecht, 2004, Springer (2006).
- ⁴³ M. D. Stoller, S. Park, Y. Zhu, J. An, and R. S. Ruoff, *Nano Lett.* **8**, 3498 (2008).
- ⁴⁴ R. Ryoo, S. H. Joo, M. Kruk, and M. Jaroniec, *Adv. Mater.* **13**, 677 (2001).